

REPORT DOCUMENTATION PAGE

Form Approved
OMB No. 074-0188

Public reporting burden for this collection of information is estimated to average 1 hour per response, including the time for reviewing instructions, searching existing data sources, gathering and maintaining the data needed, and completing and reviewing this collection of information. Send comments regarding this burden estimate or any other aspect of this collection of information, including suggestions for reducing this burden to Washington Headquarters Services, Directorate for Information Operations and Reports, 1215 Jefferson Davis Highway, Suite 1204, Arlington, VA 22202-4302, and to the Office of Management and Budget, Paperwork Reduction Project (0704-0188), Washington, DC 20503

1. AGENCY USE ONLY (Leave blank)		2. REPORT DATE December 18, 2006	3. REPORT TYPE AND DATES COVERED Final Technical (3/8/04-9/8/06)	
4. TITLE AND SUBTITLE Synthesis of Multifunctional Materials			5. FUNDING NUMBERS Grant #N00014-04-1-0347	
6. AUTHOR(S) Hadis Morkoç, Ph.D.				
7. PERFORMING ORGANIZATION NAME(S) AND ADDRESS(ES) Virginia Commonwealth University School of Engineering PO Box 843068 Richmond, VA 23284-3068			8. PERFORMING ORGANIZATION REPORT NUMBER Final Technical for #529196	
9. SPONSORING / MONITORING AGENCY NAME(S) AND ADDRESS(ES) Office of Naval Research Program Officer, Colin E. Wood ONR Code 312 875 N Randolph St, One Liberty Ctr., Arlington, VA 22203-1995			10. SPONSORING / MONITORING AGENCY REPORT NUMBER	
11. SUPPLEMENTARY NOTES				
12a. DISTRIBUTION / AVAILABILITY STATEMENT APPROVED FOR PUBLIC RELEASE			12b. DISTRIBUTION CODE	
13. ABSTRACT (Maximum 200 Words) <p>Single-crystal PbTiO₃ layers were grown on (001) SrTiO₃ substrates by molecular beam epitaxy using hydrogen peroxide as an oxidant. Phase composition and structural properties of the films were examined as a function of growth parameters. It was found that single-phase PbTiO₃ films grew epitaxially at substrate temperatures of 600°C and higher, whereas layers grown at lower temperature contained PbO inclusions.</p> <p>Growth of Pb(Zr_xTi_{1-x})O₃ (PZT) films by molecular beam epitaxy was demonstrated for the first time. Single-crystal, single-phase PZT films were grown on (001) SrTiO₃ substrates at a growth temperature of 600°C. <i>In situ</i> monitoring of the growth process by reflection high-energy electron diffraction revealed two dimensional growth mode for the end compounds of the PZT system, PbTiO₃ and PbZrO₃, and three-dimensional growth mode for PZT films of intermediate compositions.</p> <p>Epitaxial growth of PbO, TiO₂ and ZrO₂ has been achieved on MOCVD grown GaN template using oxides MBE with a reactive H₂O₂ oxygen source. In situ RHEED was used to monitor the growth in-situ. AFM was used to characterize the surface morphology of the thin PbO and ZrO₂, which show streaky, 2-D RHEED patterns.</p> <p>We have made substantial progress in the growth and characterization of PTO and PZT and also on ZrO₂ which turned out to be a very good oxide bridge layer to GaN.</p>				
14. SUBJECT TERMS GaN, Substrates, PTO, PZT, ZrO ₂			15. NUMBER OF PAGES 22	
			16. PRICE CODE	
17. SECURITY CLASSIFICATION OF REPORT Unclassified	18. SECURITY CLASSIFICATION OF THIS PAGE Unclassified	19. SECURITY CLASSIFICATION OF ABSTRACT Unclassified	20. LIMITATION OF ABSTRACT SAR	

FINAL REPORT

“Synthesis of Multifunctional Materials“

Grant #N00014-04-1-0347

Covering the period of

March 8, 2008 to September 8, 2006

Submitted to:

Office of Naval Research,
C/o Dr. Colin Wood
Code 312, Room 9-06
1 Liberty Center
875 N. Randolph St.
Arlington VA 22203
TEL: (703) 696 4218
FAX: (703) 696-2611
e mail: Woodce@onr.navy.mil
by

Hadis Morkoç
Virginia Commonwealth University
P. O. Box 843072
Richmond, VA 23284-3072

LOCATION

School of Engineering Building
601 W. Main. Richmond, VA 23220
TEL: (804) 828-0181
e mail: hmorkoc@vcu.edu

20061226006

ABSTRACT

Single-crystal PbTiO_3 layers were grown on (001) SrTiO_3 substrates by molecular beam epitaxy using hydrogen peroxide as an oxidant. Phase composition and structural properties of the films were examined as a function of growth parameters. It was found that single-phase PbTiO_3 films grew epitaxially at substrate temperatures of 600°C and higher, whereas layers grown at lower temperature contained PbO inclusions. The epitaxial relationship between the films and the substrates was $(001)\text{PbTiO}_3//(\text{001})\text{SrTiO}_3$ and $\text{PbTiO}_3[100]//\text{SrTiO}_3[100]$. No evidence of a-domains was found. Full widths at half maximum of (001) PbTiO_3 rocking curves were as low as 6-8 arcmin for 50-60 nm thick films, indicating high crystal quality of the films. From ellipsometric measurements, refractive index and band gap of PbTiO_3 were found to be 2.66 at 633 nm and 3.8 eV, respectively.

Growth of $\text{Pb}(\text{Zr}_x\text{Ti}_{1-x})\text{O}_3$ (PZT) films by molecular beam epitaxy was demonstrated for the first time. Single-crystal, single-phase PZT films were grown on (001) SrTiO_3 substrates at a growth temperature of 600°C . *In situ* monitoring of the growth process by reflection high-energy electron diffraction revealed two dimensional growth mode for the end compounds of the PZT system, PbTiO_3 and PbZrO_3 , and three-dimensional growth mode for PZT films of intermediate compositions. Layer-by-layer growth of PZT films was achieved by using a PbTiO_3 buffer layer between the SrTiO_3 substrate and PZT films. Optical properties of the films of end compositions were investigated by spectroscopic ellipsometry. Refractive index at 633 nm was found to be 2.66 for PbTiO_3 and 2.40 for PbZrO_3 . Band gap energies of PbTiO_3 and PbZrO_3 are 3.81 and 3.86 eV, in good agreement with theoretically calculated values. The P-E hysteresis loop of the 70-nm-thick PZT film was well saturated and had a square shape. The remanent polarization and the coercive field were $83 \mu\text{C}/\text{cm}^2$ and $77 \text{kV}/\text{cm}$, respectively.

Epitaxial growth of PbO , TiO_2 and ZrO_2 has been achieved on MOCVD grown GaN template using oxides MBE with a reactive H_2O_2 oxygen source. *In situ* RHEED was used to monitor the growth *in-situ*. AFM was used to characterize the surface morphology of the thin PbO and ZrO_2 , which show streaky, 2-D RHEED patterns. XRD pattern indicates that the growth orientation of these oxides are $\text{PbO} [111]//\text{GaN} [0002]$, $\text{ZrO}_2[100]//\text{GaN} [0002]$ and $\text{TiO}_2[200]//\text{GaN}[0002]$.

As the abstract indicates, we have made substantial progress in the growth and characterization of PTO and PZT and also on ZrO_2 which turned out to be a very good oxide bridge layer to GaN. Below, the details of PTO, then PZT followed by ZrO_2 are discussed.

PTO

Lead titanate ($PbTiO_3$), a ferroelectric material with perovskite structure, has received a great deal of attention owing to a unique combination of its piezoelectric, pyroelectric, dielectric, electro- and acousto-optic properties [1]. $PbTiO_3$ is a very attractive material for use in a wide variety of fields, including ultrasonic sensors, infrared detectors, electro-optic modulators, and ferroelectric random access memories. To harness the intrinsic properties of $PbTiO_3$ for device applications, however, high-quality epitaxial films are required. $PbTiO_3$ thin films have been prepared by various methods such as metal organic chemical vapor deposition (MOCVD) [2], rf magnetron sputtering [3], pulsed laser deposition [4], hydrothermal method [5], and sol-gel technique [6]. Surprisingly, molecular beam epitaxy (MBE), a modern growth technique providing high crystal perfection and precise control over material composition, has not been widely applied, except of a few reports involving ozone as an oxidizing agent [7,8]. In this contribution, we report growth of high-quality single-crystal $PbTiO_3$ layers on (001) $SrTiO_3$ substrates by MBE utilizing hydrogen peroxide as an oxidant, initially developed for ZnO [9].

Experimental details for PTO

$PbTiO_3$ layers were grown on (001) $SrTiO_3$ substrates in a Riber 3200 MBE system. The chamber was evacuated by a 1200 l/s turbo pump to a base pressure of 10^{-8} Torr. Lead (6N purity) and titanium (6N purity) were supplied from double-zone and high-temperature effusion cells, respectively. A 50% aqueous solution of hydrogen peroxide was used as a source of reactive oxygen [9]. A jet of H_2O_2/H_2O vapor was directed at the substrate through a quartz pipe connected to a leak valve.

Before loading into the chamber, single-crystal $SrTiO_3$ substrates were etched with a buffered NH_4F -HF solution, rinsed in deionized water and dried with nitrogen. Then, the substrates were loaded into the growth chamber and heated at $600^\circ C$ for 20 min under H_2O_2/H_2O pressure of 1×10^{-5} Torr. The PTO layers were grown at an H_2O_2/H_2O pressure of about 5×10^{-5} Torr, and a Pb-to-Ti flux ratio $\gg 1$. The substrate temperature, T_S , was varied in the range from 580 to $620^\circ C$ and was measured by a thermocouple located at the back of the substrate. The growth process was monitored *in situ* by reflection high-energy electron diffraction (RHEED). The thickness of the grown film varied from 24 to 65 nm.

The crystal structure of the grown layers was examined by high-resolution x-ray diffractometry (XRD) (CuK_α radiation). The surface morphology of the samples was

studied by atomic force microscopy (AFM). The thickness of the grown layers was measured with an Alpha-step 250 profilometer. Spectroscopic ellipsometric measurements were performed with variable angle spectroscopic ellipsometry (VASE) at room temperature and at incidence angles of 65, 70, and 75°.

Results and discussions for PTO

Figure 1 shows the typical RHEED patterns of a SrTiO₃ substrate and a PbTiO₃ layer grown at 600 and 620 °C along the [110] and [100] azimuths. The streaky patterns in Figures 1 (c) and (d) indicate that the growth proceeds in a two-dimensional mode. A two-fold surface reconstruction was observed along the [110] direction (Figure 1 (d)). Surface roughness of the PbTiO₃ films measured by AFM varied from 1.3 to 2 nm.

Figure 2 illustrates the effect of the growth temperature and metal flux on the film composition. The XRD data indicate that the film grown at 580°C consists of a mixture of PbTiO₃ and PbO phases (Fig. 2 (a)). The undesirable PbO can be removed by *ex situ* post-growth annealing of the films. It should be mentioned, however, that the post-growth annealing leads also to pronounced surface roughening, which deteriorates the quality of the layers. The films grown at higher temperatures are single-phase and *c*-axis oriented. Only (00*l*) reflections of PbTiO₃ and of SrTiO₃ are visible in the θ -2 θ

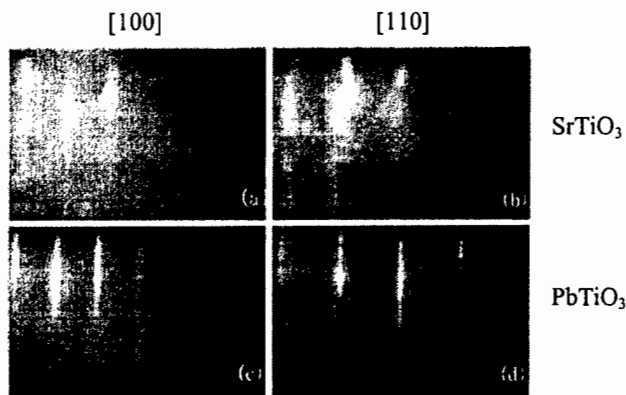


Figure 1. Representative RHEED patterns of (a) and (b) an SrTiO₃ substrate and (c) and (d) a PbTiO₃ layer, respectively.

scans for the films grown at 600°C (Figure 2 (b)). However, (*h*00) reflections of PbTiO₃ should coincide with (00*l*) reflections from the SrTiO₃ substrate. So, to detect *a*-domains possibly present in the films, rocking curves of SrTiO₃ (001) reflections were measured. No evidence of *a*-domains was found, which can be explained by the fact that all our films were thinner than the critical thickness for the 90° domain formation (100-150 nm [2,10]).

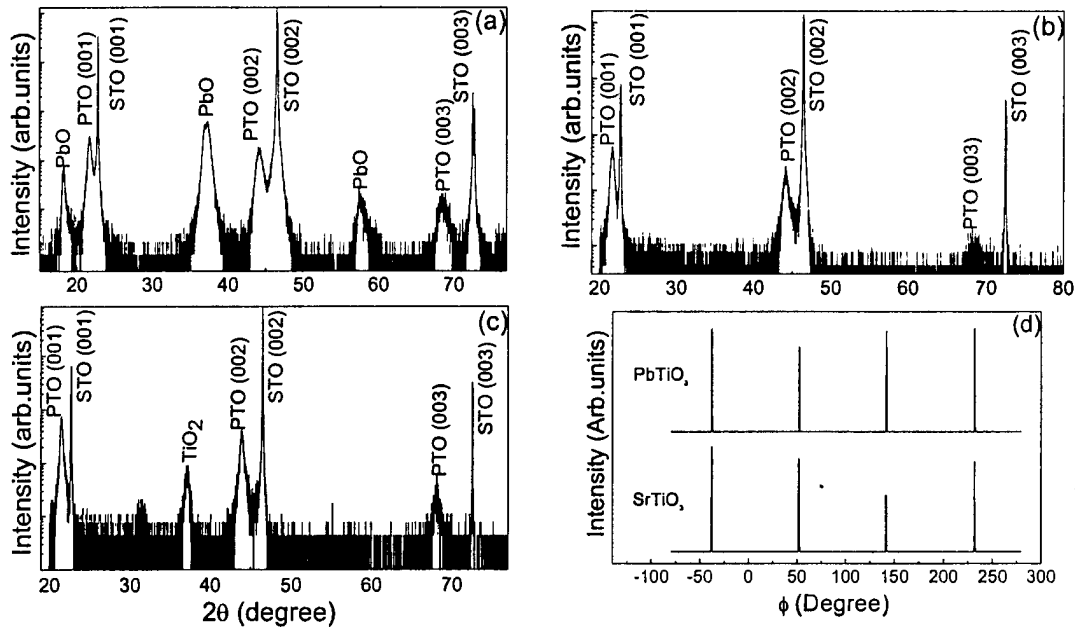


Figure 2. XRD θ - 2θ scans for PbTiO_3 (PTO) films grown on SrTiO_3 (STO) substrates at temperature of (a) 580°C , (b) 600°C , (c) at 600°C and increased metal fluxes, peroxide pressure being the same; and (d) Phi-scan for (101) planes of SrTiO_3 substrate and PbTiO_3 layer.

Figure 2 (c) shows the θ - 2θ scan for a film grown at a substrate temperature of 600°C , but with increased Ti and Pb fluxes (Pb/Ti flux ratio and $\text{H}_2\text{O}_2/\text{H}_2\text{O}$ pressure were the same as for the samples shown in Figures (a) and (b)). One can see that the film grown at higher metal flux contains the TiO_2 phase in addition to PbTiO_3 . This result is similar to that obtained by Theis *et al.* [7,8], who have reported that, despite excess Pb supply, TiO_2 phase is formed under low ozone pressures due to insufficient Pb oxidation. Taking into account that oxidation of Ti is more favorable because of the higher binding energy of Ti-O bonds [11], the appearance of TiO_2 can be attributed to the fact that available oxidant pressure was insufficient to oxidize increased amount of Pb. However, our finding indicates that the real situation is probably even more complicated. When a PbO film grows at the same Pb flux, substrate temperature, and $\text{H}_2\text{O}_2/\text{H}_2\text{O}$ pressure, the same amount of peroxide is sufficient to provide efficient oxidation of much larger amounts of Pb. Therefore, the growth rate of PbO is five times larger than that of PbTiO_3 (60 nm/h for PbO as compared to 12 nm/h for PbTiO_3). The phase composition of the PbO films was verified by XRD. To clarify this issue, we evaluated the probability of incorporation of Pb atoms into PbTiO_3 and PbO. Incorporation coefficient, I , was calculated as

$$I = J_{arr}/J_{inc}, \quad (1)$$

where J_{arr} and J_{inc} are fluxes of Pb atoms arrived to the surface and incorporated into a growing film, respectively. J_{arr} is equal to the product of Pb deposition rate and Pb atomic density ($3.28 \times 10^{22} \text{ cm}^{-3}$), and J_{inc} is equal to the product of PbTiO_3 or PbO growth rate and the density of Pb sites in PbTiO_3 or PbO lattice. The coefficients of Pb incorporation

into PbTiO_3 and PbO were estimated to be 0.017 and 0.136, respectively. One can see that the incorporation of Pb into PbTiO_3 is lower than that into PbO by a factor of 8, indicating complicated nature of the growth mechanism of PbTiO_3 . We can presume that such factors as density and configuration of dangling bonds on the surface, surface reconstruction, presence of Ti , and growth mode (three-dimensional growth of PbO versus layer-by-layer mode for PbTiO_3) can influence the incorporation of Pb . Much remains to be learned about the growth mechanism.

Figure 2 (d) shows Φ scans for (101) reflections of a SrTiO_3 substrate and a PbTiO_3 film grown at 600°C . One can see that both the layer and the substrate show four peaks 90° apart from one another. The peaks from the film and the substrate are at the same angular positions, indicating the epitaxial relationship $(001)\text{PbTiO}_3// (001)\text{SrTiO}_3$ and $\text{PbTiO}_3[100]//\text{SrTiO}_3[100]$. Lattice parameters c and a were calculated from 2θ positions of symmetrical (001) and asymmetrical (101) reflections, respectively. For our PbTiO_3 films in the thickness range of 24 - 65 nm, c -parameters were found to vary from 4.10 to 4.13 Å, and a -parameters from 3.91 to 3.93 Å. The values of c for all our films are less than the reported bulk c -parameter ($c = 4.156$ Å [12]), whereas a -parameters are larger than the bulk value ($a = 3.905$ Å [12]), indicating that the films are under in-plane tensile strain. Since the lattice mismatch between PbTiO_3 and SrTiO_3 is very small, the residual strain arise most probably during sample cooling after growth due to the difference in thermal expansion coefficient between the film and the substrate or/and to the volume change during transformation from the cubic to tetragonal PbTiO_3 phase. Can we be more quantitative by figuring out the strain due to cooling and or phase change. Full width at half maximum (FWHM) of XRD rocking curves measured for the (001) reflection decreased from 16 arcmin to 6 arcmin as the film thickness increased from 24 to 65 nm, pointing to a very good alignment in the growth direction. The value of 6 arcmin is comparable to the best values reported for MOCVD [2] and hydrothermal [5] PbTiO_3 films.

Pseudodielectric function of PbTiO_3 was measured by spectroscopic ellipsometry in the spectral range from 1 to 6 eV. The sample structure was modeled as consisting of a rough surface layer, a main PbTiO_3 layer, and a substrate, and the dielectric function of the main PbTiO_3 layer was estimated using the parametric optical constant (POC) model [13]. The pseudodielectric functions and modeled dielectric functions match very well and are not discernible because of the excellent fitting, as seen from Figure 3, which shows the pseudodielectric function and fitted dielectric function for a PbTiO_3 film grown on a SrTiO_3 substrate.

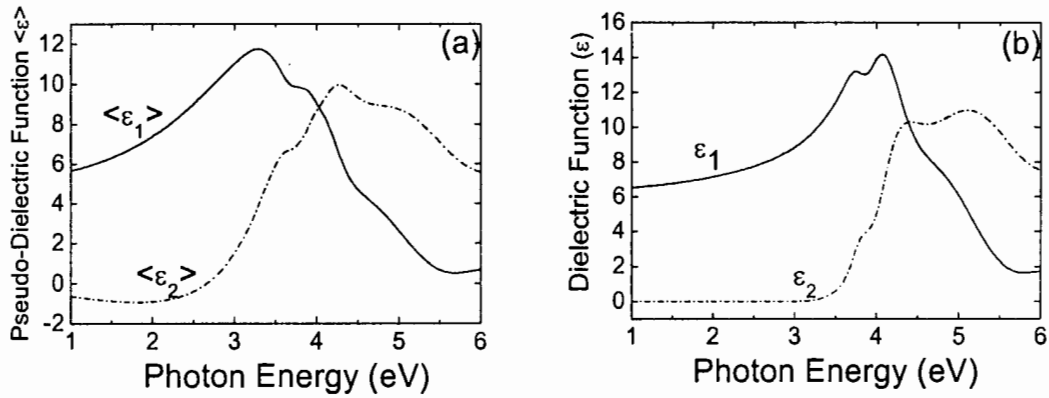


Figure 3. (a) Pseudodielectric function ($\langle \epsilon \rangle = \langle \epsilon_1 \rangle + i\langle \epsilon_2 \rangle$) of the PbTiO₃ film grown on (100) PbTiO₃ substrate. Solid and dash-and-dotted curves represent the real and imaginary parts, respectively. (b) Fitted dielectric function ($\epsilon = \epsilon_1 + i\epsilon_2$) of the PbTiO₃.

The thickness of this layer was fitted to be 35.5 ± 0.9 nm, and the surface roughness layer, 4.0 ± 0.3 nm. Figure 4 (a) presents fitted complex refractive index of the 35-nm-thick PbTiO₃ layer. Note that the dielectric function is the square of the complex refractive index $\epsilon = (n+ik)^2$. The value of the refractive index is 2.66 at 633 nm (1.96 eV), which is very close to the bulk value of 2.668 [14], indicating excellent crystal quality of the material.

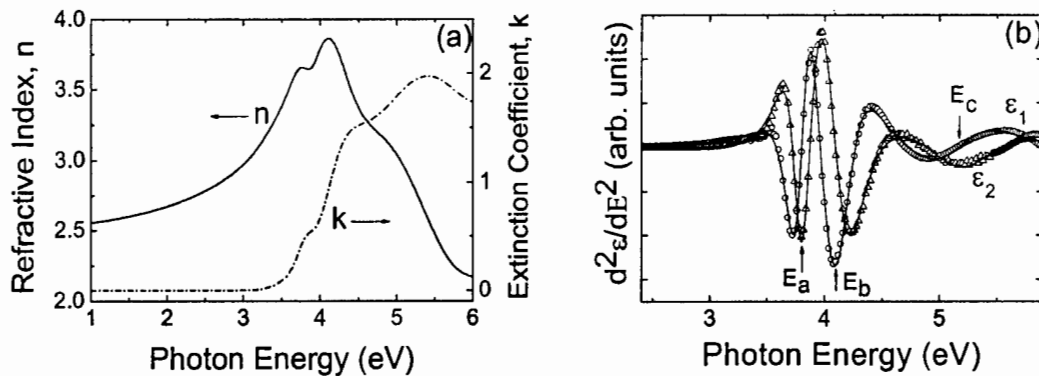


Figure 4. (a) Fitted complex refractive index ($n+ik$) of PTO layer. (b) Plot of the second derivative of the PbTiO₃ dielectric function (symbols) and their fits (solid curve) of using SCP model. The fitted band-gap energies (E_a , E_b , and E_c) are marked with arrows.

In order to estimate the band-gap parameters of PbTiO₃, we took the second derivative of the dielectric functions and fitted them using the standard critical point (SCP) model [15]. The SCP model assumes simple parabolic dispersion relation for direct interband transitions and provides accurate critical point parameters (band gap energies). Figure 4 (b) presents the second derivative of the dielectric functions and their fit using the SCP model. The fitted band-gap energies (E_a , E_b , and E_c) are marked with arrows and listed in Table I, along with the theoretical values found previously by Lee *et al.* [16], who

calculated the band structure of PbTiO_3 by using local density approximation (LDA) method. According to their calculation, there are four interband transitions in PbTiO_3 in the visible-ultra-violet spectral range. They estimated the transition amplitudes and concluded that only three transitions are substantial. As shown in the Table I, the ellipsometrically estimated band gap values are in good agreement with those calculated theoretically.

Table I. Experimental and theoretical PbTiO_3 band gap parameters.

Band-gap energy	Transition	Experimental (this work)	Theory [16]
E_a	$X_{5v} \rightarrow X_{3c}$	3.81 ± 0.01 eV	3.78 eV
E_b	$X_{4v} \rightarrow X_{1c}$	4.11 ± 0.01 eV	4.00 eV
E_c	$X_{5v} \rightarrow X_{1c}$	5.2 ± 0.1 eV	4.93 eV

Conclusions for PTO

High-quality PbTiO_3 films were grown on SrTiO_3 substrates by MBE utilizing H_2O_2 as an oxidant. Conditions for the MBE growth of single-phase, single crystalline PbTiO_3 films were found: the films grown at 580°C contained lead oxide inclusions, whereas single-phase layers grew at 600 and 620°C with the epitaxial relationship $(001)\text{PbTiO}_3//((001)\text{SrTiO}_3$ and $\text{PbTiO}_3[100]//\text{SrTiO}_3[100]$. The low values of FWHM of (001) rocking curves (down to 6 arc min) are indicative of high crystal quality of the grown layers. The lattice constants of PbTiO_3 determined from XRD data indicate the films to be under in-plane tensile strain. Refractive index and band gap energies of the PbTiO_3 films were determined with variable angle spectroscopic ellipsometry in the spectral range of 1 to 6 eV. Refractive index was found to be 2.66 at 633 nm, which is close to the bulk value. The experimentally determined band gap values agree well with the band structure calculations performed previously.

PZT

Introduction for PZT

Due to their large piezoelectric coefficient, electrical polarization, and electromechanical coupling factor, ferroelectric $\text{Pb}(\text{Zr}_x\text{Ti}_{1-x})\text{O}_3$ (or PZT) thin films are of considerable interest for a wide range of applications, such as gate material for ultrasonic sensors, infrared detectors, ferroelectric field effect transistors, and nonvolatile ferroelectric random access memory devices [17]. Piezoelectric and ferroelectric properties of this material have been studied extensively as a function of composition. It was demonstrated that the piezoelectric coefficient, relative permittivity, and remanent polarization peaked

near the morphotropic phase boundary [18]. To exploit the unique properties of PZT for device applications, high quality single-crystal PZT films are required. However, most of the studies have been done on ceramic samples, whereas the properties of single-crystal thin films can differ drastically from those for ceramics [19] and depend strongly on film orientation [20, 21, 22, 23].

PZT thin films have been prepared by various methods such as metal organic chemical vapor deposition (MOCVD) [20,21, 22], rf magnetron sputtering [24, 25, 26], pulsed laser deposition [27, 28], and sol-gel technique [29, 30]. To the best of our knowledge, molecular beam epitaxy (MBE), a modern growth technique providing high crystal perfection and precise control over material composition, has not been used for the fabrication of PZT films up to now. In this contribution, we report on the growth of high quality PZT films by peroxide MBE and study of their structural, optical, and ferroelectric characteristics.

Experimental details for PZT

PZT layers were grown on (001) SrTiO₃ substrates in Riber 3200 MBE system. The chamber was evacuated by a 1200 l/s turbo pump to a base pressure of 10⁻⁸ Torr. Aqueous solution of hydrogen peroxide (H₂O₂) was employed as a source of reactive oxygen [31], 6N-purity lead and titanium were supplied from double-zone and high-temperature effusion cells, respectively. Due to the very low equilibrium pressure of metal Zr, zirconium tetra (Zr-t) butoxide was chosen as the metal-organic precursor, and 6N-purity Ar was used as a carrier gas. Before loading into the chamber, SrTiO₃ substrates were etched with a buffered NH₄F-HF solution, rinsed in deionized water and dried with nitrogen. Then, the substrates were loaded into the growth chamber and heated at 600°C for 20 min under H₂O₂/H₂O pressure of 1x10⁻⁵ Torr. PZT layers 30 to 70 nm thick were grown at an H₂O₂/H₂O pressure of about 5 x 10⁻⁵ Torr, a substrate temperature of 600°C, and a Pb-to-Ti flux ratio >>1. Zr/Ti ratio in the PZT films was varied by changing a flow rate of the carrier gas. The growth process was monitored *in situ* by reflection high-energy electron diffraction (RHEED). Surface morphology of the films was examined by atomic force microscopy (AFM). Phase composition and structural properties of the films were examined by x-ray diffraction (XRD). The thickness of the grown layers was measured with an Alpha-step 250 profilometer. Spectroscopic ellipsometric measurements were performed with the use of variable angle spectroscopic ellipsometry (VASE) at room temperature and incidence angles of 65, 70, and 75°.

Results and discussions for PZT

Figure 1 shows RHEED patterns of the end compounds of the Pb(Zr_xTi_{1-x})O₃ system, PbTiO₃ and PbZrO₃, taken after growth. The streaky RHEED patterns indicate that the growth of these compounds proceeded in two-dimensional mode. However, when PZT films were grown directly on SrTiO₃, spotty RHEED patterns were observed in the beginning of the growth due to three-dimensional growth mode and rough surface morphology (Figure 2 (b)). The spotty RHEED patterns of the PZT films became worse with time, transforming into partially ring pattern characteristic of textured polycrystalline films, as illustrated in Figure 2 (c). To overcome this problem, we introduced PbTiO₃ buffer layers between the SrTiO₃ substrates and PZT films. As seen

from Figure 3, the PZT layer grown on the $\text{PbTiO}_3/\text{SrTiO}_3$ structure show streaky RHEED patterns characteristic of two-dimensional growth and smooth film surface. Surface morphology of the PZT films grown through the buffer layers was examined by AFM. Figure 3 (d) shows $1 \times 1 \mu\text{m}$ AFM image of the PZT film surface. Steps and terraces are visible on the surface. The step height is about 4 nm, which is comparable to the unit cell of PZT, evidencing layer-by-layer growth mode. The root mean square of surface

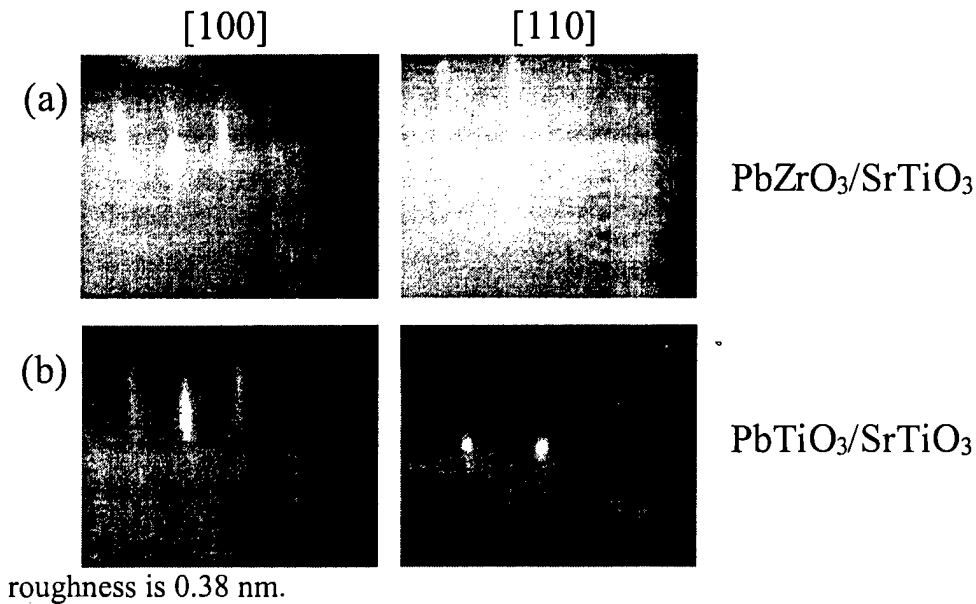


Figure 1. Representative RHEED patterns of (a) PbTiO_3 and (b) PbZrO_3 films grown on SrTiO_3 substrates.

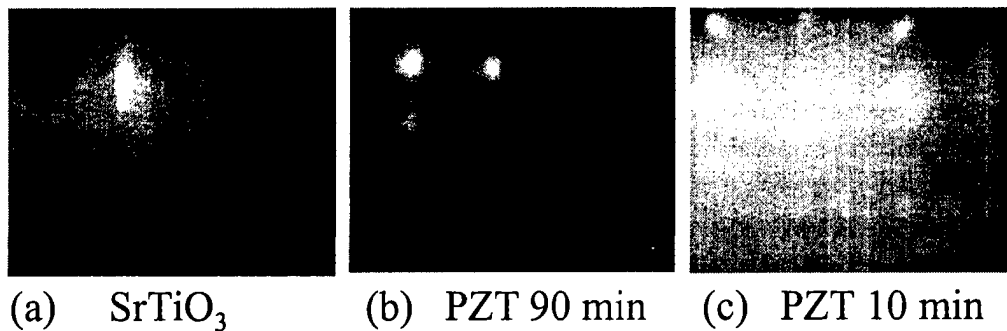
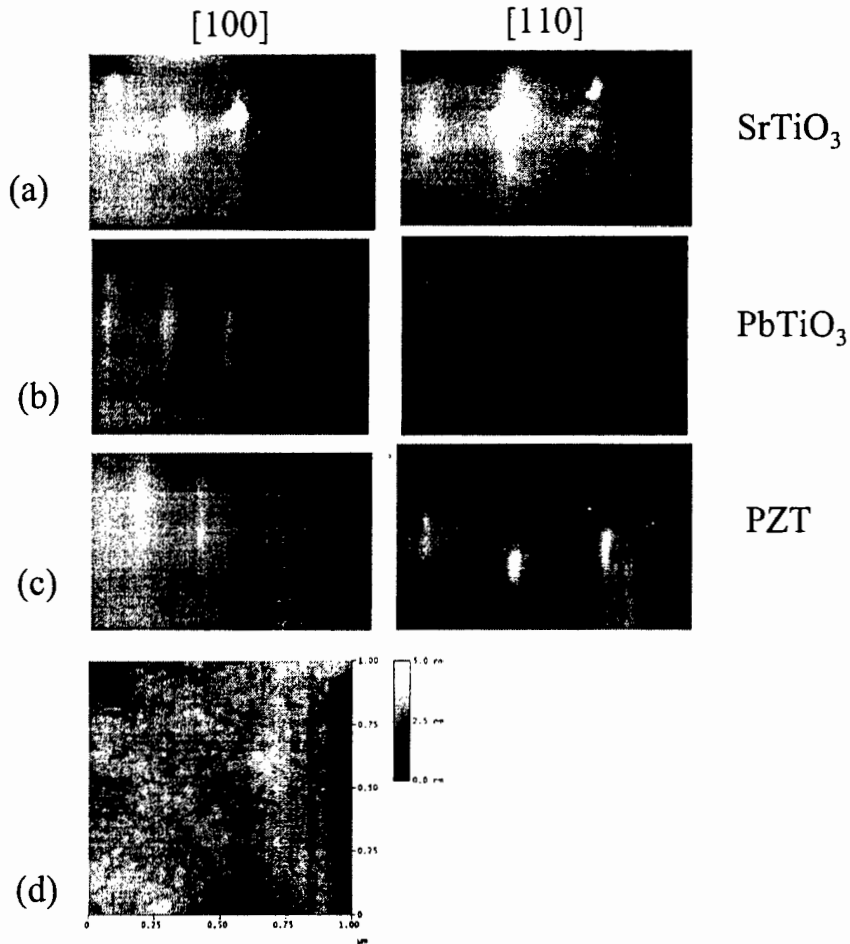


Figure 2. RHEED patterns taken along $[100]$ azimuth from (a) SrTiO_3 substrate, (b) PZT layer after 10 min growth, and (c) PZT layer after 90 min growth.

As evidenced from XRD data, the PZT films of all investigated compositions are single-phase, c-axis oriented. Figure 4 presents θ - 2θ scans of a $\text{PZT}/\text{PbTiO}_3/\text{SrTiO}_3$ and $\text{PbZrO}_3/\text{SrTiO}_3$ structures. Only $(00l)$ reflections of the substrate and the layers are seen in the scans. As mentioned in the Experimental section, the Zr content in the PZT films was varied by changing flow rate of the carrier gas and was roughly estimated from

growth rates of end compounds, PbTiO_3 and PbZrO_3 , assuming the same incorporation



probabilities for the constituting components. It should be mentioned, that the estimation of PZT film composition from XRD data is a severe problem, because our films are very thin (below 100 nm) and not fully relaxed, so thickness and residual strain resulted from lattice mismatch, difference in thermal expansion coefficients, and volume change during phase transformation have significant influence on the lattice parameters. Therefore, another technique, such as x-ray fluorescence spectrometry, secondary ion

Figure 3. RHEED patterns of (a) SrTiO_3 substrate, (b) PbTiO_3 buffer layer, and (c) a 30-nm-thick PZT layer taken after growth, and (d) AFM image of this PZT film, vertical scale is 5 μm .

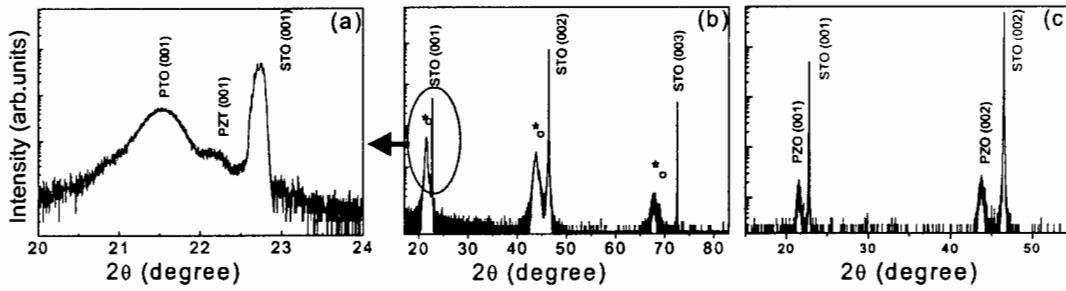


Figure 4. XRD θ - 2θ scans for a PZT film grown on a PbTiO_3 (PTO) layer on SrTiO_3 (STO) substrates: (a) first-order reflections and (b) wider angular range for the same scan (PbTiO_3 and PZT reflections are marked by an asterisk and a circle, respectively); and (c) for a PbZrO_3 layer on SrTiO_3 substrate.

mass spectrometry, or Rutherford backscattering, will be applied to determine exact film compositions.

Optical properties of PbTiO_3 and PbZrO_3 films were investigated by spectroscopic ellipsometry. The ellipsometric measurements as well as results for PbTiO_3 films are described in more detail in Ref [32]. Refractive index at 633 nm is found to be 2.66 for PbTiO_3 and 2.40 for PbZrO_3 , which is consistent with the literature data [33]. The experimentally determined band gap values 3.81 eV for PbTiO_3 and 3.86 eV for PbZrO_3 are in good agreement with theoretical values calculated previously by Lee *et al.* [34]. Optical properties of the films of intermediate PZT compositions are now under examination.

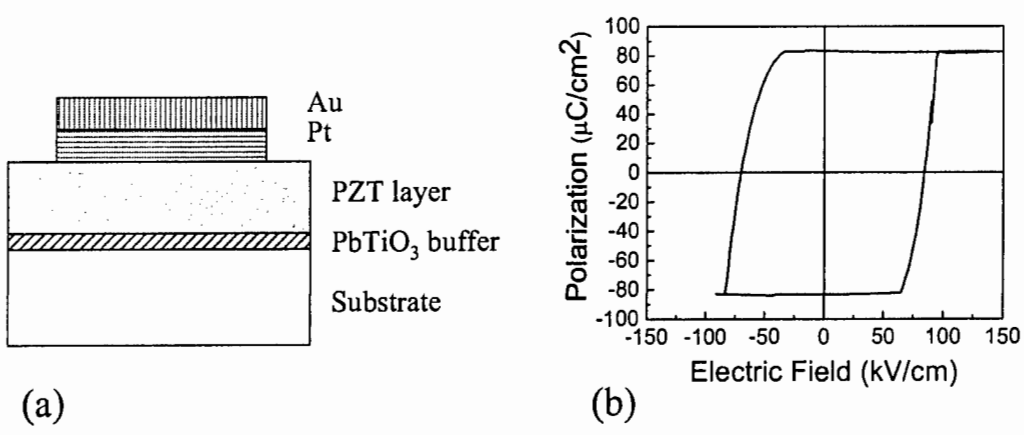


Figure 5. (a) Schematic sketch of the capacitor test structure. (b) P-E hysteresis curve for the 70-nm-thick PZT film.

To investigate ferroelectric properties, PZT films were grown on conductive Nb-doped SrTiO_3 substrates. Capacitor device structures were fabricated as shown in Figure 5 (a). Au/Pt top electrodes 30nm/30nm in thickness, 300 μm in diameter were deposited by e-beam evaporation. The polarization *versus* applied electric field (P-E) characteristics

were measured at room temperature with a Radiant Technologies Precision LC ferroelectric test system. Figure 5 (b) shows a P-E hysteresis loop for the 70-nm-thick PZT film. The loop is well-saturated and square in shape, with high remanent polarization of $83 \mu\text{C}/\text{cm}^2$, and the coercive field of $77 \text{ kV}/\text{cm}$. It should be mentioned, however, that current-voltage characteristics of this structure shows high leakage current of $5.7 \times 10^{-2} \text{ A}/\text{cm}^2$ for applied bias of 2 V. The reason of the high leakage is now under investigation.

Conclusions for PZT

Single crystal, single-phase PZT films were successfully grown on (001) SrTiO_3 substrates by peroxide MBE. It is found that the end compounds of the $\text{Pb}(\text{Zr}_x\text{Ti}_{1-x})\text{O}_3$ system, PbTiO_3 and PbZrO_3 , grow on SrTiO_3 in two dimensional mode, whereas the growth of PZT films of intermediate compositions proceeds in three-dimensional mode. The use of PbTiO_3 buffer layer between the SrTiO_3 substrate and PZT results in layer-by-layer growth of PZT films. From ellipsometric measurements, values of refractive index and band gap energy were found for the end compositions of the PZT system. Square-shaped P-E hysteresis loop was observed for the 70-nm-thick PZT film, with a remanent polarization of $83 \mu\text{C}/\text{cm}^2$. The large value of the remanent polarization evidences that the MBE-grown PZT films show a great promise for device applications.

ZrO₂

Introduction for ZrO₂

Lead titanate based thin films, such as PbTiO_3 (PTO) and $\text{Pb}(\text{Zr,Ti})\text{O}_3$ (PZT) show a great promise for a wide variety of applications such as integrated piezoelectric devices³⁵, pyroelectric infrared sensors³⁶, nonvolatile memory³⁷, optical waveguide devices,³⁸ and electro-optic modulators.³⁹ The integration of these perovskite oxides with existing semiconductors such as GaN is of particular interest which makes use of intrinsic characteristics of ferroelectric thin films, in the form, *e.g.*, PZT gated GaN based ferroelectric MODFET⁴⁰.

Experimental details for ZrO₂

Due to the very different crystal structure between the PZT and GaN (perovskite for PZT while hexagonal for GaN), a bridge layer must be inserted for their successful integration. PbO , ZrO_2 and TiO_2 are interesting materials by themselves and each of them has their applications in different fields. In the presented work, these oxides are of particular interest due to the factor that they are relative compounds of PZT and therefore could be promising candidates for the integration of PZT and GaN, as they have been used in the literatures as the buffer layer for PZT growth^{41, 42, 43}. We present a study of PbO , TiO_2 and ZrO_2 grown by molecular beam epitaxy (MBE) as candidates for bridge layers for the integration of PZT with GaN. The GaN template used in this experiment was prepared by

metal-organic chemical vapor deposition. The MBE system used in this study is a Riber 3200 customized for oxides growth. Ti flux was provided by a high-temperature Knudsen cell and Pb was evaporated from a double-zone Knudsen cell. Metal-organic Zr precursor, Zr-t butoxide, was kept in a bubbler heated by a water bath and argon was used as the carrier gas. In order to overcome the shortcomings of the conventional oxygen plasma sources such as possible surface damage by high-energy particle and degradation of plasma sources due to the high reactivity of oxygen radicals, a highly reactive H_2O_2 source was employed. 50% aqueous solution of H_2O_2 was placed in a stainless steel bubbler heated by water bath. The flow rate of the H_2O_2 was controlled by the leak valve and the pressure was monitored by the vacuum gauge. A schematic of our growth chamber is shown in figure 1.

Results and discussions for ZrO_2

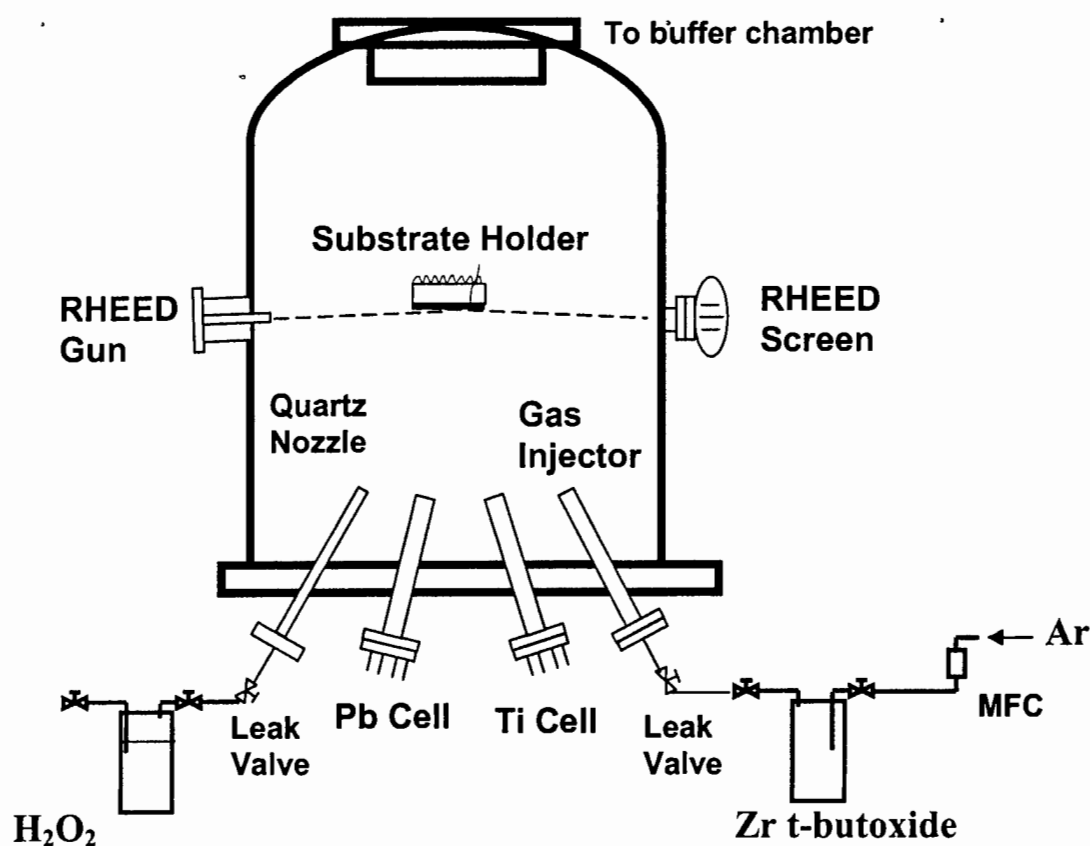


Figure.1 Schematic drawing of our Riber 32 system for oxides growth

Different approaches were used for epitaxial growth of PbO , TiO_2 , and ZrO_2 was performed using: epitaxy of TiO_2 was performed at $600^\circ C$. A two step growth was found to be needed for ZrO_2 : growth of low temperature buffer at $300^\circ C$ to minimize the oxidation of GaN template followed by annealing at $750^\circ C$ and high temperature growth at $700^\circ C$. For both TiO_2 and ZrO_2 growth, the H_2O_2 pressure was kept between 1.5 and 3.0×10^{-5} Torr. The situation is different for the growth of PbO , which is more volatile

than both TiO_2 and ZrO_2 . Therefore, a reduced temperature (550°C) and high H_2O_2 pressure ($\sim 5.0 \times 10^{-5}$ Torr) was adopted.

RHEED was used to monitor the growth in-situ, and figure 2-4 show the patterns for the PbO , ZrO_2 and TiO_2 , respectively.

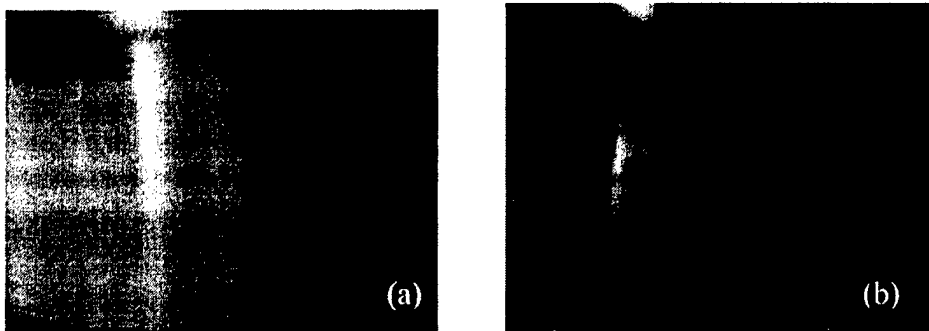


Figure.2 RHEED pattern of PbO grown on GaN (a) parallel to GaN $(11\bar{2}0)$ direction (b) 15 degrees rotated from GaN $(11\bar{2}0)$ direction

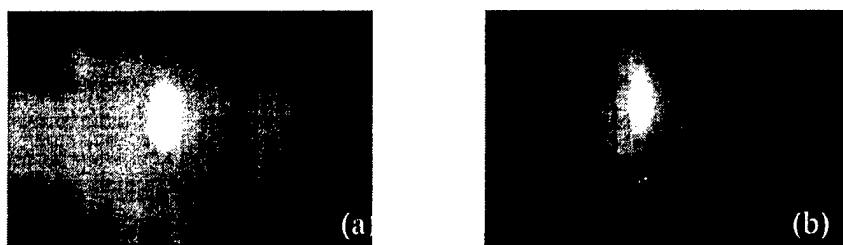


Figure.3 RHEED pattern of (a) ZrO_2 low temperature buffer layer (b) high temperature layer both taken along (011) direction

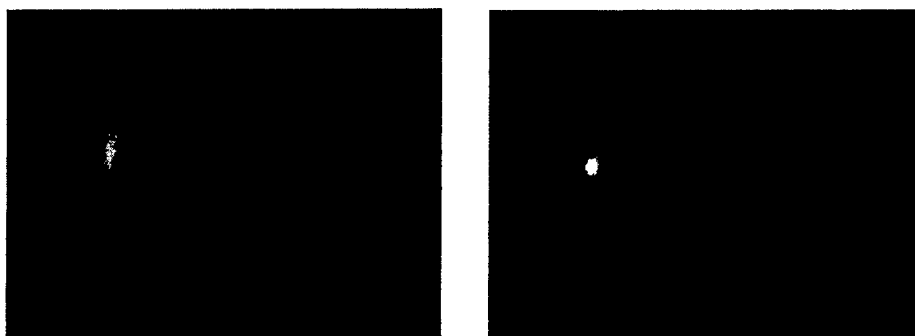
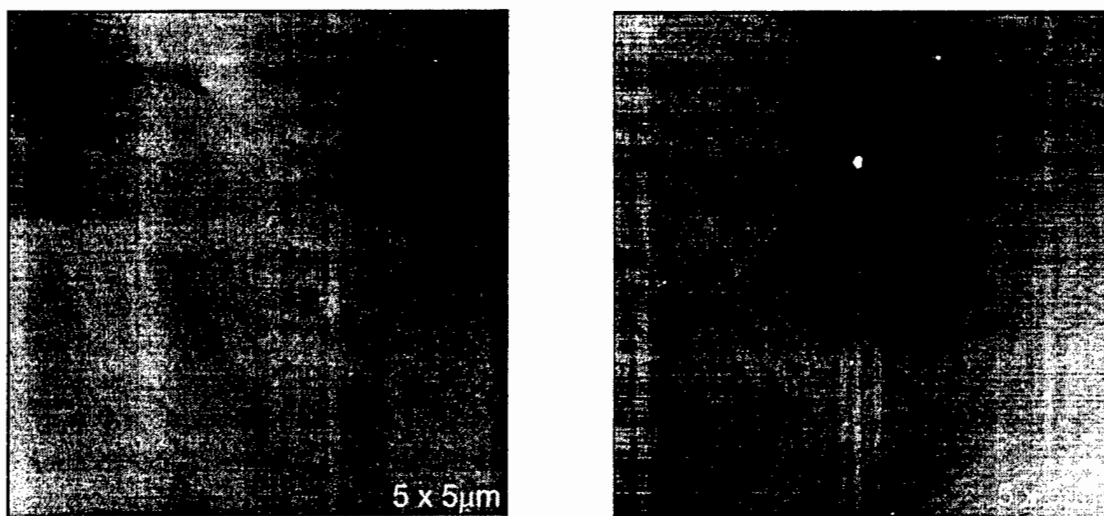


Figure.4 RHEED pattern of TiO_2 along GaN $(11\bar{2}0)$ (a) 10-nm-thick layer (b) 120-nm-thick layer.

As seen from figure 2, PbO shows a streaky pattern indicating 2 dimensional (2D) mode. In the case of ZrO_2 , since the reactive species cannot acquire enough thermal energy at low growth temperatures, the ZrO_2 grown at low temperature exhibits a 3D RHEED

pattern, which turn into a 2-D streaky one upon annealing at 750°C and maintained during the high temperature growth. The situation is somewhat reverse for the TiO₂ growth: After 5 minutes growth the pattern of GaN diminished and replaced by the pattern of TiO₂. It is noticeable that the TiO₂ epitaxial on GaN started in a 2D mode. With the increase of the thickness the growth mode switched to 3D.

AFM was performed to study the surface morphology of epitaxially grown 10nm thick ZrO₂ and 20nm thick PbO layers, and the images are shown in figure 5. In both cases, the AFM images are indicative of smooth and uniform oxides. These oxides films are contiguous, and some features of the atomic step from the MOCVD GaN template remain observable.

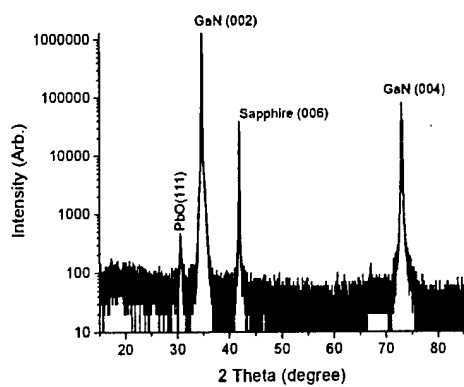


(a)

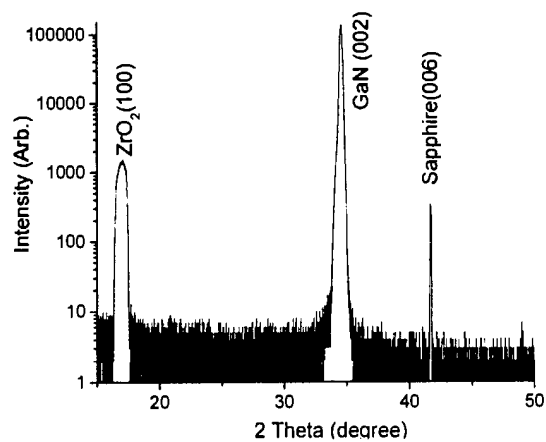
(b)

Figure.5 AFM images of (a) PbO on GaN (b) ZrO₂ on GaN. The image size is 5μm by 5μm and vertical scale is 5nm.

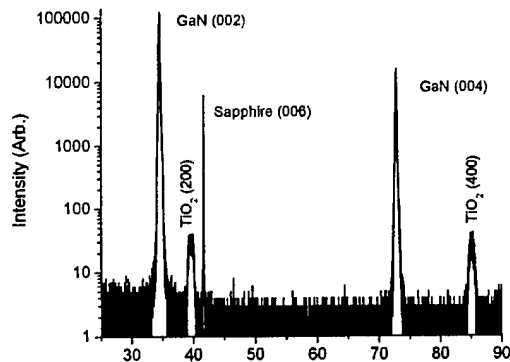
In order to study crystal structure and phase composition of the prepared oxide layers, XRD measurements have been performed and the patterns are shown in figure 6(a). For the 20-nm-thick PbO, only (111) reflections of orthorhombic PbO can be observed along with the GaN the sapphire substrate. The peaks of TiO₂ grown on GaN are consistent with (200) reflections of orthorhombic phase (see figure 6(b)). Figure 6(c) shows the θ -2 θ XRD pattern of a 30nm thick ZrO₂/GaN, which is indicative of (100)-oriented monoclinic ZrO₂.



(a)



(c)



(b)

Figure.6 XRD theta-2theta pattern of (a) PbO(111)/GaN(0002) (b) ZrO₂(100)/GaN (0002) (c) TiO₂ (200)/GaN(0002)

Conclusions for ZrO₂

In summary, PbO, TiO₂ and ZrO₂ have been grown epitaxially on GaN/c-Al₂O₃ substrates by oxides MBE using H₂O₂ as a source of reactive oxygen. In situ RHEED was used to monitor the growth in-situ shows 2-D growth for PbO and ZrO₂, and a 2-D to 3-D transition for TiO₂. AFM was used to characterize the surface morphology of the thin PbO and ZrO₂ and indicates a contiguous feature. XRD pattern indicates that the growth orientation of these oxides are PbO [111]//GaN [0002], ZrO₂[100]//GaN [0002] and TiO₂[200]//GaN[0002].

Publications resulting from ONR support

H. Lee, Y. -S. Kang, S-J Cho, Y.-I Alivov, N. Izyumskaya, and Hadis Morkoç, "Multi-functional perovskite oxides and their applications: a review", *Critical Reviews in Solid State and Materials Sciences*, by invitation only, submitted.

Y.-I Alivov, N. Izyumskaya, F. Agra, M. Wu, and Hadis Morkoç, "Multifunctional oxides: ferroelectrics, ferromagnetics, multiferroics and high κ - materials", *Applied Physics Reviews*, by invitation only - about to be submitted.

H. Lee, T. D. Kang, Y. S. Kang, S-J Cho, and H. Morkoç, "Visible-Deep UV Dielectric Functions and Electronic Band Structure of Lead Zirconate Titanate Thin Films", March 06 APS meeting, Baltimore Maryland

Hosun Lee, Youn Seon Kang, Sang-Jun Cho, Hadis Morkoç, and Tae Dong Kang, "Visible-ultraviolet spectroscopic ellipsometry of Lead Zirconate Titanate thin films", *Appl. Phys. Lett.* **86**, 262902 (2005).

Hosun Lee, Youn Seon Kang, Sang-Jun Cho, Bo Xiao, Hadis Morkoç, Tae Dong Kang, Jingbo Li and Su-Huai Wei, Paul Snyder, and J. T. Evans, "Dielectric Function and Electronic Band Structure of Lead Zirconate Titanate thin films", *J. Appl. Phys.* **98**, 094108 (2005)

Youn-Seon Kang, Jinqiao Xie, Qian Fan, Sang-Jun Cho, Yong-Tae Moon, Bo Xiao, Norio Onojima, Daniel Johnstone, Hadis Morkoç, Hosun Lee, and Young-Soo Park, "Ferroelectric PZT/AlGaIn/GaN field effect transistors", *SPIE Opto 06*, Jan 06 San Jose CA. *Proceedings of SPIE*, Vol. 6121, 6121OS1-5 (2006)

Youn-Seon Kang, Qian Fan, Bo Xiao, Ya. I. Alivov, Jinqiao Xie, Norio Onojima, Sang-Jun Cho, Yong-Tae Moon, Hosun Lee, D. Johnstone, Hadis Morkoç, and Young-Soo Park, "Fabrication and current-voltage characterization of ferroelectric PZT/AlGaIn/GaN field effect transistor", *Appl. Phys. Lett.* vol.88, no.12, pp. 123508-1-3, 20 March 2006

Tae Dong Kang, Ghill Soo Lee, Ho Suk Lee, Hosun Lee, Youn Seon Kang, Sang-Jun Cho, Bo Xio, Hadis Morkoç, and Paul G. Snyder, "Infrared Ellipsometric Study on PZT Thin Films", *Journal of the Korean Physical Society*, Vol. 49, No. 4, pp. 1604-1610 October 2006

V. Avrutin, N. Izyumskaya, Xing Gu, Ü. Özgür, B. Xiao, Tae Dong Kang, Hosun Lee, and H. Morkoç, "Growth of high quality $\text{Pb}(\text{Zr}_x\text{Ti}_{1-x})\text{O}_3$ films by peroxide MBE and their optical and structural characteristics", Fall MRS 06 meeting

Xing Gu, Natalia Izyumskaya, Vitaly Avrutin, Tae Dong Kang, Hosun Lee and Hadis Morkoç, "High quality epitaxial growth of PbTiO_3 by MBE using H_2O_2 as the oxygen source", *Appl. Phys. Letts.*, Vol. 89, n 12, p 122912, (2006),

V. Avrutin, N. Izyumskaya, Xing Gu, Ü. Özgür, B. Xiao, Tae Dong Kang, Hosun Lee, and H. Morkoç, "Growth of high quality $\text{Pb}(\text{Zr}_x\text{Ti}_{1-x})\text{O}_3$ films by peroxide MBE and their optical and structural characteristics", Fall MRS 06 meeting.

N. Izyumskaya, V. Avrutin, Xing Gu, Ü. Özgür, Tae Dong Kang, Hosun Lee, and H. Morkoç, "Structural and optical properties of PbTiO_3 grown on STO substrate by peroxide MBE", Fall MRS 06 meeting.

Xing Gu, Jinqiao Xie, Serguei Chevtchenko, Natalia Izyumskaya, Vitaly Avrutin, and Hadis Morkoç, "Epitaxial growth of ZrO_2 on GaN by MOMBE for high dielectric material applications", Fall MRS 06 meeting.

Xing Gu, Natalia Izyumskaya, Vitaly Avrutin, Jinqiao Xie, Serguei Chevtchenko, and Hadis Morkoç, "AlGaIn/GaN MOS transistors using crystalline ZrO_2 as gate dielectric", SPIE Photonic West-Opto 07 20-25 January 2007

T. D. Kang, Hoseok Lee, and Hosun Lee, G. Xing, N. Izyumskaya, V. Avrutin, and H. Morkoç, "Dielectric Functions and Band Gaps of PbTiO_3 , PbZrO_3 , and $\text{PbZr}_{1-x}\text{Ti}_x\text{O}_3$ Grown on SrTiO_3 Substrates by Using Peroxide Molecular Beam Epitaxy", American Physics Society March meeting 07 Denver CO.

References

- ¹. A.J. Moulson, J.M. Herbert, *Electroceramics*, Second ed, Wiley, New York, 2003.
- ². Z. Li, M. Foster, D. Guo, H. Zhang, G. R. Bai, P. M. Baldo, and L. E. Rehn, *Appl. Phys. Lett.* **65**, 1106 (1994).
- ³. D.M. Kim, C.B. Eom, V. Nagarajan, J. Ouyang, R. Ramesh, V. Vaithyanathan, and D.G. Schlom, *Appl. Phys. Lett.* **88**, 142904 (2006).
- ⁴. Kiho Lee and Sunggi Baik, *Appl. Phys. Lett.* **86**, 202901 (2005).
- ⁵. T. Morita and Y. Cho, *Jpn. J. Appl. Phys., Part 1* **43**, 6535 (2004).
- ⁶. H. D. Chen, K. R. Udayakumar, C. J. Gaskey, and L. E. Cross, *Appl. Phys. Lett.* **67**, 3411 (1995).
- ⁷. C. D. Theis and D. G. Schlom, *J. Cryst. Growth* **174**, 473 (1997).
- ⁸. C. D. Theis, J. Yeh, D. G. Schlom, M. E. Hawley, and G. W. Brown, *Thin Solid Films* **325**, 107 (1998).
- ⁹. N. Izyumskaya, V. Avrutin, W. Schoch, A. El-Shaer, F. Reuss, Th. Gruber, and A. Waag, *J. Cryst. Growth* **269**, 356 (2004).
- ¹⁰. M. de Keijser, D.M. de Leeuw, P.J. van Veldhoven, A.E.M. De Veirman, D.G. Neerincx, and G.J.M. Dormans, *Thin Solid Films* **266**, 157 (1995).
- ¹¹. *CRC Handbook of Chemistry and Physics*, ed. D.R. Lide, 86th ed. (CRC Press, Boca Raton, 2005-2006).
- ¹². A. M. Glazer and S. A. Mabud, *Acta Cryst. B* **34**, 1065 (1978).
- ¹³. B. Johs, C. M. Herzinger, J. H. Dinan, A. Cornfeld, and J. D. Benson, *Thin Solid Films* **313/314**, 137 (1998).
- ¹⁴. P. D. Thacher, *Appl. Optics* **16**, 3210 (1977).
- ¹⁵. P. Lautenschlager, M. Garriga, L. Viña, and M. Cardona, *Phys. Rev. B* **36**, 4821 (1987), and references therein.
- ¹⁶. Hosun Lee, Youn-Seon Kang, Sang-Jun Cho, Bo Xiao, Hadis Morkoç, Tae Dong Kang, Jingbo Li, Su-Hwai Wei, P. J. Snyder, and J. T. Evans, *J. Appl. Phys.* **98**, 094108 (2005) and references therein.

-
- ¹⁷ J.F. Scott and Paz de Araujo, *Science* **246**, 1400 (1989).
- ¹⁸ B. Jaffe, J.W.R. Cook, and H. Jaffe, *Piezoelectric Ceramics* (Academic, New York, 1971).
- ¹⁹ D.-J. Kim, J.-P. Maria, A. I. Kingon, and S. K. Streiffer, *J. Appl. Phys.* **93**, 5568 (2003).
- ²⁰ T. Oikawa, M. Aratani, H. Funakubo, K. Saito, and M. Mizuhira, *J. Appl. Phys.* **95**, 3111 (2004).
- ²¹ Shintaro Yokoyama, Yoshihisa Honda, Hitoshi Morioka, Shoji Okamoto, Hiroshi Funakubo, Takashi Iijima, Hirofumi Matsuda, Keisuke Saito, Takashi Yamamoto, Hirotake Okino, Osami Sakata, Shigeru Kimura, *J. Appl. Phys.* **98**, 094106 (2005).
- ²² Kuniharu Nagashima, Masanori Aratani, and Hiroshi Funakubo, *J. Appl. Phys.* **89**, 4517 (2001).
- ²³ Xiao-hong Du, Jiehui Zheng, Uma Belegundu, and Kenji Uchino, *Appl. Phys. Lett.* **72**, 2421 (1998).
- ²⁴ Hosun Lee, Youn-Seon Kang, Sang-Jun Cho, Bo Xiao, Hadis Morkoç, Tae Dong Kang, Jingbo Li, Su-Hwai Wei, P. J. Snyder, and J. T. Evans, *J. Appl. Phys.* **98**, 094108 (2005).
- ²⁵ D.M. Kim, C.B. Eom, V. Nagarajan, J. Ouyang, R. Ramesh, V. Vaithyanathan, and D.G. Schlom, *Appl. Phys. Lett.* **88**, 142905 (2006).
- ²⁶ S. Kalpat and K. Uchino, *J. Appl. Phys.* **90**, 2703 (2001).
- ²⁷ Kiho Lee and Sunggi Baik, *Appl. Phys. Lett.* **86**, 202901 (2005).
- ²⁸ T. J. Zhu, L. Lu, and C. V. Thompson, *J. Crystal Growth* **273**, 172 (2004).
- ²⁹ H. D. Chen, K. R. Udayakumar, C. J. Gaskey, and L. E. Cross, *Appl. Phys. Lett.* **67**, 3411 (1995).
- ³⁰ A. Gruverman, W. Cao, S. Bhaskar, and S. K. Dey, *Appl. Phys. Lett.* **84**, 5351 (2004).
- ³¹ N. Izyumskaya, V. Avrutin, W. Schoch, A. El-Shaer, F. Reuss, Th. Gruber, and A. Waag, *J. Cryst. Growth* **269**, 356 (2004).
- ³² N. Izyumskaya, V. Avrutin, Xing Gu, Ü. Özgür, Tae Dong Kang, Hosun Lee, and H. Morkoç, *ibid.*

-
- ³³ M. P. Moret, M. A. C. Devillers, K. Wörhoff, and P. K. Larsen, *J. Appl. Phys.* **92**, 468 (2002).
- ³⁴ Hosun Lee, Youn-Seon Kang, Sang-Jun Cho, Bo Xiao, Hadis Morkoç, Tae Dong Kang, Jingbo Li, Su-Hwai Wei, P. J. Snyder, and J. T. Evans, *J. Appl. Phys.* **98**, 094108 (2005).
- ³⁵ C. A. Paz de Araujo and G. W. Taylor, *Ferroelectrics* **116**, 215 (1991)
- ³⁶ Jyh-Jier Ho, Y. K. Fang, K. H. Wu, W. T. Hsieh, C. W. Chu, C. R. Huang, M. S. Ju, and C. P. Chang, *IEEE Elect. Dev. Lett.*, **19** (6), 189, (1998)
- ³⁷ R. E. Newnham and G. R. Ruschau, *J. Am. Ceram. Soc.* **74**, 463 (1991)
- ³⁸ A. Essahlaoui, A. Roemer, A. Boudrioua, E. Millon, J.C. Loulergue, *Optical Mater.* **24**, 465 (2003)
- ³⁹ C. E. Land, *J. Am. Ceram. Soc.* **72**, 2059 (1989).
- ⁴⁰ Y. S. Kang, Q. Fan, B. Xiao, Y. I. Alivov, J. Q. Xie, N. Onojima, S. J. Cho, Y. T. Moon, H. Lee, D. Johnstone, H. Morkoç, Y. S. Park, *Appl. Phys. Lett.* **88**, 123508 (2006)
- ⁴¹ S. Hiboux and P. Muralt, *J. Euro. Ceramic Soc.* **24** 1593 (2004)
- ⁴² W. Gong, J. Li, X. Chu, Z. Gui and L. Li, *Acta Mater.* **52** 2787 (2004)
- ⁴³ C. Zhu, Y. Chentao, L. Bo and Y. Bangchao, *Mater. Lett.* **60** 1559 (2006)